

Three-dimensional tidal sand waves

PAOLO BLONDEAUX† AND GIOVANNA VITTORI

Department of Civil, Environmental and Architectural Engineering – University of Genoa
Via Montallegro 1, 16145 Genova, Italy

(Received 13 May 2008 and in revised form 10 September 2008)

The process which leads to the formation of three-dimensional sand waves is investigated by means of a stability analysis which considers the time development of a small-amplitude bottom perturbation of a shallow tidal sea. The weakly nonlinear interaction of a triad of resonant harmonic components of the bottom perturbation is considered. The results show that the investigated resonance mechanism can trigger the formation of a three-dimensional bottom pattern similar to that observed in the field.

1. Introduction

The bottom topography of many shallow tidal seas is often characterized by the presence of periodic morphological patterns of different spatial scales which range from a few centimetres (ripples) to tens of kilometres (sand banks) (Sleath 1984; Belderson, Johnson & Kenyon 1982). The sand waves are medium-scale bed forms, being characterized by wavelengths of the order of hundreds of metres. Sometimes, the sand waves are almost two-dimensional, at other times, these bottom patterns turn out to be three-dimensional and regular enough to identify a longitudinal and a transverse wavelength. Figure 1 (adapted from Knaapen *et al.* 2001) shows an example of a three-dimensional bottom topography where three-dimensional sand waves are superimposed on long bed waves and sand banks. A qualitative analysis of the bottom topography shows that the crests of the sand waves are almost orthogonal to the local tidal current. Moreover, their wavelength turns out to be a few hundred metres and the ratio between the longitudinal wavelength (the wavelength in the direction of the tidal current) and the transverse wavelength is of order one.

In the last decade, in order to investigate the mechanism which gives rise to sand waves, theoretical analyses have been developed which are based on a linear stability approach and consider the time development of bottom perturbations of ‘small’ (strictly infinitesimal) amplitude (see e.g. Hulscher 1996; Gerkema 2000; Besio *et al.* 2003, 2006). Previous studies of sand wave appearance often assume the tidal flow to be unidirectional and consider two-dimensional bottom perturbations, with crests orthogonal to the direction of the tidal current. The results obtained allow us to identify the conditions leading to the appearance of two-dimensional sand waves and to predict the wavelength of these bottom forms. However, in order to explain the appearance of three-dimensional bottom forms like those shown in figure 1, it is necessary to consider not only the growth of three-dimensional bottom perturbations, but also the nonlinear interaction of the different harmonic components of the bottom perturbation. In the past, an analysis which considers the time development of

† Email address for correspondence: bix@dicat.unige.it

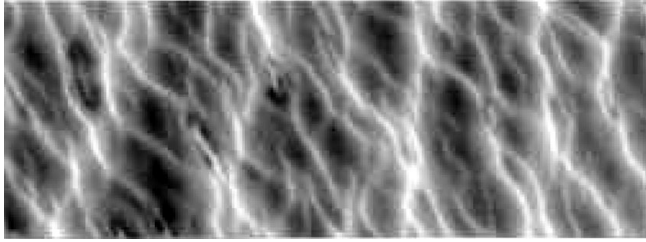


FIGURE 1. Bottom topography measured in the Noordhinder area, North Sea (adapted from Roos 2004 after Knaapen *et al.* 2001). The area of the measured bathymetry has a length of about 5 km and a width of about 2 km and the tidal current oscillates approximatively from left to right of the figure and vice versa. The water depth increases from light to dark grey.

three-dimensional bottom perturbations of the sea bottom and their possible interaction was performed by Vittori & Blondeaux (1992) to investigate the mechanism which gives rise to the brick-pattern ripples observed at the bottom of sea waves (Sleath 1984). The analysis was revisited by Roos & Blondeaux (2001) to study the so-called tile ripples (Allen 1984).

To explain the appearance of three-dimensional tidal sand waves, we investigate the time development of three-dimensional bottom perturbations of the flat bottom of shallow seas forced by elliptical tidal currents. The analysis follows the main idea of Vittori & Blondeaux (1992) and considers the weakly nonlinear interaction of three harmonic components of the bottom perturbation. The first component is a bottom waviness characterized by crests orthogonal to the major axis of the tidal ellipse, which is supposed to be aligned with the x -axis, and by a longitudinal wavenumber α . The other two components have a longitudinal wavenumber which is equal to $\alpha/2$ and opposite non-vanishing transverse wavenumbers γ and $-\gamma$, respectively. However, whereas in Vittori & Blondeaux's analysis (1992) the investigated bed forms (ripples) have a wavelength of $O(10\text{ cm})$ and affect only a thin boundary layer close to the bottom where the flow regime is assumed to be laminar, in the present case, sand waves have a length scale larger than the local water depth and affect the whole water column where a turbulent flow is present. Therefore, different hydrodynamic and morphodynamic models are introduced which require different solution procedures. It follows that in Vittori & Blondeaux (1992), the linear analysis gives rise to a range of unstable wavenumbers which tend to vanish as the parameters of the problem tend to their critical values. On the other hand, in the present case, a finite range of unstable wavenumbers exists because the critical conditions are given by the disappearance of the sediment transport rate. This result implies that a somewhat heuristic approach should be followed to work out the solution. To keep the analysis as simple as possible, we introduce a constant eddy viscosity, to close the turbulence problem, and a simple sediment transport predictor which relates the amount of sediment transported by the tidal current to the fluid velocity close to the bottom, to quantify the sediment transport rate.

The procedure used in the rest of the paper is as follows. In the next section, we briefly describe the main ingredients of the hydrodynamic problem and introduce the sediment transport parameterization. In § 3.1, we determine the basic flow and study the linear interaction of the tidal current with an arbitrary bottom perturbation. Then, in § 3.2, we investigate the weakly nonlinear resonant interaction of a triad of harmonic components of the bottom perturbation and we determine the conditions leading to the appearance of bottom configurations similar to those observed in the field and shown in figure 1.

2. Formulation of the problem

A shallow sea of small depth h^* is considered and a Cartesian coordinate system is introduced such that the x^* - and y^* -axes are horizontal with the x^* -axis aligned with the major axis of the tidal ellipse and the z^* -axis is vertical pointing upwards with the origin at the still-water level (hereinafter a star denotes dimensional quantities). The seabed is supposed to be made of cohesionless sediment of uniform size d^* and density ρ_s^* . To simplify the problem, only a tidal constituent of angular frequency ω^* is considered.

The hydrodynamics is described by continuity and momentum equations. The flow regime is turbulent and viscous effects are neglected. An exhaustive analysis of turbulence properties in tidal currents is provided in Soulsby (1983). Field measurements show that the Boussinesq hypothesis can be safely used to model Reynolds stresses, and a scalar kinematic eddy viscosity ν_T^* can be introduced which is then assumed to be constant. A time-independent eddy-viscosity model provides a fair description of the phenomenon because it fails mainly at flow reversal, when the tidal current is very weak and the transport of any quantity, and in particular of sediment particles, tends to vanish (Gerkema 2000). The constant value of the eddy viscosity ν_T^* is obtained following Besio *et al.* (2003), i.e. by equating the constant value of the eddy viscosity to the depth-averaged value of an empirical parabolic eddy-viscosity distribution. It turns out that $\nu_T^* = kU_0^*h_0^*/(6C)$, where $k = 0.4$ is the von Kármán constant, U_0^* is the maximum value of the depth-averaged velocity during the tidal cycle, h_0^* is the average water depth and C is a friction factor, which depends only on the dimensionless roughness size z_r^*/h_0^* , since the Reynolds number of the flow is assumed to be large. Standard formulae for steady currents can be used to evaluate C , e.g. $C = 5.75 \log_{10}(11h_0^*/z_r^*)$. A constant eddy-viscosity model provides an approximate, but still acceptable, description of the flow, provided the no-slip condition at the bottom is replaced by a partial slip condition (Gerkema 2000). Finally, we neglect Coriolis effects, since they play a major role in the process which leads to the formation of sand banks, controlling the orientation of their crests with respect to the tidal ellipse, but they can be safely neglected in the study of sand wave dynamics (Gerkema 2000). On defining the following dimensionless variables

$$(x, y, z) = \frac{(x^*, y^*, z^*)}{h_0^*}, \quad t = t^*\omega^*, \quad \mathbf{v} = (u, v, w) = \frac{\mathbf{v}^*}{U_0^*} = \frac{(u^*, v^*, w^*)}{U_0^*},$$

$$p = \frac{p^*}{\rho^*\omega^*h_0^*U_0^*}, \quad (2.1)$$

(ρ^* is the sea water density, t^* is time, (u^*, v^*, w^*) are the velocity components along the x^* -, y^* -, z^* -axes, p^* is pressure), the flow equations become

$$\nabla \cdot \mathbf{v} = 0, \quad \frac{1}{\hat{r}} \frac{\partial \mathbf{v}}{\partial t} + (\mathbf{v} \cdot \nabla) \mathbf{v} = \frac{g^*h_0^*}{U_0^{*2}} \mathbf{k} - \frac{1}{\hat{r}} \nabla p + \hat{\Delta} \nabla^2 \mathbf{v}, \quad (2.2)$$

where \mathbf{k} is the unit vector along the z -axis and g^* is acceleration due to gravity. In (2.2), two dimensionless parameters appear:

$$\hat{r} = U_0^*/(\omega^*h_0^*), \quad \hat{\Delta} = k/(6C). \quad (2.3)$$

The parameter \hat{r} can be interpreted as the ratio between the amplitude of horizontal fluid displacement and the local depth, while $\hat{\Delta}$ is a bottom friction parameter. The hydrodynamic problem is then complemented by appropriate boundary conditions. Following Besio *et al.* (2006), we introduce the rigid-lid approximation and, at the free surface described by $z = 0$, we force the pressure to be equal to the atmospheric

pressure and the vanishing of the shear stresses. At the sea bottom, the constant eddy-viscosity assumption requires a partial slip condition

$$\frac{\partial \mathbf{u}_{\parallel}}{\partial n} = s \mathbf{u}_{\parallel} \quad \text{at } z = -h, \quad (2.4)$$

where \mathbf{u}_{\parallel} is the velocity evaluated at the bottom and parallel to it and n is the coordinate normal to it. Moreover, $h = h^*/h_0^*$ is the dimensionless local water depth and $s = s^*h_0^*$ is a stress parameter which is fixed by forcing the shear stress acting on the bed to be equal to $\rho^*(U_0^*/C)^2$. It turns out that $s = 6/(kC - 2)$. Finally, the velocity component normal to the bottom should vanish

$$\mathbf{v} \cdot \nabla h = 0 \quad \text{at } z = -h. \quad (2.5)$$

The morphodynamics is governed by the sediment continuity equation which simply states that convergence (or divergence) of the sediment flux must be accompanied by a rise (or fall) of the bed profile. A simple analysis of the different terms appearing in the sediment continuity equation shows that the bottom changes taking place during the tidal cycle are quite small and, to observe significant variations, it is necessary to wait a large number of tidal cycles. In other words, the bottom profile significantly changes on a time scale (the morphodynamic time scale) which is much longer than the hydrodynamic time scale (the tide period) and $\partial h/\partial t$ can be neglected in (2.5). If the small oscillations of the bottom profile taking place during the tidal cycle around the mean position are neglected, it is possible to consider the sediment transport rate $(\overline{Q}_x, \overline{Q}_y)$ per unit width averaged over the tide period and to force the sediment balance on the net flux of sediment. This procedure leads to

$$\frac{\partial h}{\partial T} = \frac{\partial \overline{Q}_x}{\partial x} + \frac{\partial \overline{Q}_y}{\partial y}, \quad (2.6)$$

where $(Q_x, Q_y) = (Q_x^*, Q_y^*)/\sqrt{(\rho_s^*/\rho^* - 1)g^*(d^*)^3}$ are the instantaneous dimensionless volumetric sediment transport rates per unit width in the x - and y -directions, respectively, and an overbar denotes the time average over the tide period. Moreover, in (2.6), the slow morphodynamic time scale,

$$T = \tau^* \sqrt{(\rho_s^*/\rho^* - 1)g^*d^{*3}} / [(1 - p_{or})h_0^{*2}], \quad (2.7)$$

is introduced. In (2.7), p_{or} is the sediment porosity. To estimate (Q_x, Q_y) , we use a formula, similar to that used in previous studies of sand wave appearance, such that the sediment flux depends on the horizontal fluid velocity $\mathbf{u}_b = (u, v, 0)$ evaluated at the averaged sea bed

$$(Q_x, Q_y) = \mathcal{Q}(|\mathbf{u}_b| - u_c)^3 (\mathbf{u}_b/|\mathbf{u}_b| - \beta \nabla h) H(|\mathbf{u}_b| - u_c), \quad (2.8)$$

where H indicates the Heaviside step function, u_c is the critical value of the velocity such that for $|\mathbf{u}_b|$ smaller than u_c no sediment moves and (Q_x, Q_y) vanishes. The constants \mathcal{Q} , u_c and β can be estimated by comparing (2.8) with standard empirical sediment transport predictors. In particular, in the present study, the following values have been used which have been fixed comparing (2.8) with Meyer-Peter & Muller formula and comparing the slope effects with those suggested by Seminara (1998),

$$\mathcal{Q} = 8 \left[\frac{\sqrt{\psi} \hat{r}}{C} \left(1 + \frac{2}{3c_1(2+c_1)} \right) \right]^3, \quad u_c = c_2 \frac{C}{\hat{r}} \sqrt{\frac{0.05}{\psi}}, \quad \beta = -\frac{0.15C^2}{\psi \hat{r}^2}, \quad (2.9)$$

where $c_1 = -1 + \sqrt{1 + 2/s}$, $c_2 = 3c_1(2 + c_1)/[3c_1(2 + c_1) + 2]$. Moreover, in (2.9), the mobility number $\psi = (\omega^* h_0^*)^2 / [(\rho_s^* / \rho^* - 1)g^* d^*]$ is introduced. Let us point out that, for fixed values of sea and sediment characteristics and considering a semi-diurnal tide, the constants \mathcal{Q} , u_c and β depend only on the parameter \hat{r} , which is a measure of the strength of the tidal current and turns out to control the stability of the bed configuration.

3. The time development of bottom perturbations of small amplitude

Small perturbations of the flat bottom are considered and the bottom profile can be thought as being described by the superposition of different spatial harmonic components.

3.1. The perturbation time development: the linear regime

In the linear regime, each component of the bottom perturbation evolves independently from the others and the problem can be solved for the generic spatial component

$$h = 1 - \epsilon [A(t)e^{i(\alpha x + \gamma y)} + \text{c.c.}], \quad (3.1)$$

where $\epsilon A(t)$ is the dimensionless amplitude of the generic component which is periodic in the x - and y -directions with wavenumbers α and γ , respectively, and $\epsilon \ll 1$. The small value of ϵ allows for the solution of the hydrodynamic problem formulated in §2 to be expanded in the form

$$(u, v, w, p) = \left(u_0, v_0, w_0, \frac{\sqrt{g^*}}{\omega^* \sqrt{h_0^*}} P_0 \right) + \epsilon [(u_1, v_1, w_1, \hat{r} P_1) A(t) e^{i(\alpha x + \gamma y)} + \text{c.c.}] + O(\epsilon^2), \quad (3.2)$$

where the dynamic pressure $P = p - g^* z / (U_0^* \omega^*)$ is introduced. Then, assuming that the averaged water depth h_0^* is much smaller than the length L^* of the tidal wave and neglecting terms of order h_0^*/L^* , the local tidal flow over a flat bottom can be determined in the form

$$(u_0, v_0, w_0) = \frac{|\lambda_1| (2c_3 \cosh(\lambda_1 z) - i)}{2|2c_3 \sinh \lambda_1 - i\lambda_1|} \left(1, i \frac{b}{a}, 0 \right) e^{-iz} + \text{c.c.}, \quad (3.3)$$

where $\lambda_1 = (-1 + i)/\sqrt{2\hat{\Delta}\hat{r}}$, $c_3 = is/[2(s \cosh \lambda_1 + \lambda_1 \sinh \lambda_1)]$, and b/a is the ratio between the minor and major axes of the tidal ellipse. When (3.2) is substituted into the flow problem formulated in §2 and terms of order ϵ are considered, the following set of linear equations for u_1, v_1, w_1 and p_1 is derived:

$$i\alpha u_1 + i\gamma v_1 + \frac{\partial w_1}{\partial z} = 0, \quad (3.4)$$

$$\begin{aligned} & i(\alpha u_0 + \gamma v_0)(u_1, v_1, w_1) + w_1 \left(\frac{\partial u_0}{\partial z}, \frac{\partial v_0}{\partial z}, 0 \right) \\ & = - \left(i\alpha, i\gamma, \frac{\partial}{\partial z} \right) P_1 + \hat{\Delta} \left(\frac{\partial^2}{\partial z^2} - \alpha^2 - \gamma^2 \right) (u_1, v_1, w_1) \end{aligned} \quad (3.5)$$

subject to the following boundary conditions

$$\frac{\partial}{\partial z}(u_1, v_1) = 0, \quad -P_1 + 2\hat{\Delta} \frac{\partial w_1}{\partial z} = 0, \quad w_1 = 0 \quad \text{at} \quad z = 0, \quad (3.6)$$

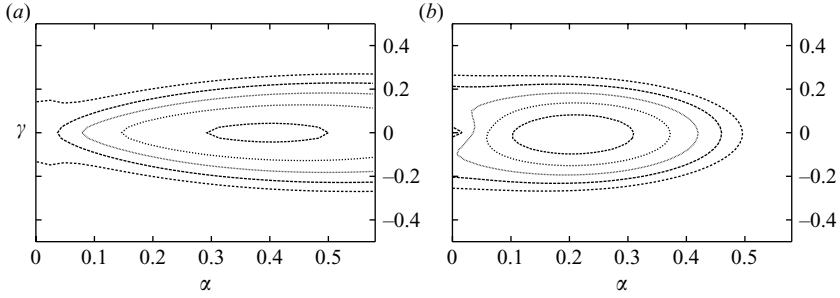


FIGURE 2. Growth rate Γ_R of the bottom perturbation predicted by the linear analysis and plotted versus α and γ for $\hat{r} = 110$, $\hat{\Delta} = 2.87 \times 10^{-3}$. Only positive isolines are displayed with $\Delta\Gamma_R = 0.5 \times 10^{-4}$. (a) $b/a = 0.2$, the maximum value of Γ_R is located at $(\alpha, \gamma) \simeq (0.39, 0.0)$, (b) $b/a = 0.9$, the maximum value of Γ_R is located at $(\alpha, \gamma) \simeq (0.20, 0.0)$.

$$\left(\frac{\partial}{\partial z} - s\right)(u_1, v_1) = -\frac{\partial}{\partial z}\left(\frac{\partial}{\partial z} - s\right)(u_0, v_0), \quad w_1 = 0 \quad \text{at} \quad z = -h. \quad (3.7)$$

The terms proportional to $dA(t)/dt$ which would appear in (3.5) have been neglected since the bottom time development takes place on the morphodynamic time scale T which is much slower than the hydrodynamic time scale t . Moreover, because of the large values assumed by the parameter \hat{r} for field conditions, it is possible to neglect also the local acceleration term which is proportional to $1/\hat{r}$ and negligible in the whole water column (Blondeaux & Vittori 2005). Therefore, in (3.4) and (3.5), the time t is just a parameter and the solution procedure used by Blondeaux & Vittori (2005) can be employed to determine (u_1, v_1, w_1, p_1) . For field conditions, the parameter $\hat{\Delta}$ is of order $1/\hat{r}$. However, the stress terms are retained in (3.5) because they are not negligible within a boundary layer close to the bottom and the solution procedure takes them into account without the need to split the fluid domain into an inviscid region and a boundary layer. Then, the expansion of the sediment transport rate

$$(Q_x, Q_y) = (Q_{x0}, Q_{y0}) + \epsilon A(t)(Q_{x1}, Q_{y1})e^{i(\alpha x + \gamma y)} + \text{c.c.} + O(\epsilon^2), \quad (3.8)$$

can be readily evaluated by using (2.8) and the computed flow field. Then, it is possible to evaluate the tide averaged values $(\overline{Q_x}, \overline{Q_y})$ following the procedure outlined in Tambroni & Blondeaux (2008) which takes into account the discontinuous behaviour of the sediment transport rate. Since the algebra, though straightforward, is lengthy and tedious, we omit the details which are given in Vittori & Blondeaux (2008). The equation which provides the time development of the amplitude of the bottom perturbation follows from the sediment continuity:

$$\frac{dA(T)}{dT} = i(\alpha Q_{x1} + \gamma Q_{y1})A(T) = \Gamma(\alpha, \gamma, \hat{r})A(T), \quad (3.9)$$

where, for a semi-diurnal tide and fixed values of the sea and sediment characteristics, the growth rate Γ is a complex quantity which depends on the wavenumbers of the harmonic component of the bottom perturbation and on the parameter \hat{r} . The solution of (3.9),

$$A(T) = A_0 \exp[\Gamma T], \quad (3.10)$$

shows that the growth or the decay of the bottom perturbation is controlled by the real part Γ_R of Γ . Figure 2(a) shows Γ_R as a function of α and γ for values of the parameters chosen in order to reproduce the climate and sediment

characteristics of a typical site in the North Sea ($\omega^* = 1.41 \times 10^{-4} \text{ s}^{-1}$, $U_0^* = 0.39 \text{ m s}^{-1}$, $b/a = 0.2$, $h_0^* = 25 \text{ m}$, $z_r^* = 2.5 \text{ cm}$, $d^* = 0.2 \text{ mm}$). The bed forms which tend to appear are characterized by crests orthogonal to the major axis of the tidal ellipse since the maximum value of Γ_R is attained for vanishing values of γ . Moreover, the perturbation component characterized by the maximum amplification rate, i.e. the component which will dominate the bottom configuration for long times, is characterized by $\alpha \simeq 0.39$. This wavenumber corresponds to a dimensional wavelength of about 400 m, a value similar to the wavelengths observed in the field which fall between 100 m and 800 m (Hulscher 1996). The e-folding time, which provides the order of magnitude of the morphodynamic process, turns out to be $O(10^3)$ years. Even though the time scale of sand wave development is very long (e.g. the field data of Knaapen & Hulscher (2002) show that dredged sand waves take about 10 years to recover only partially), the estimated time scale appears somewhat long. However, note that tidal currents stronger than that presently considered (in the North Sea U_0^* can be larger than 1 m s^{-1}) can decrease the order of magnitude of the e-folding time.

When the value of \hat{r} is decreased, a critical value \hat{r}_c is found such that for \hat{r} smaller than \hat{r}_c , no sediment moves and the bottom perturbations do not grow. For the chosen parameters, the value of \hat{r}_c turns out to be about 82 which corresponds to $U_0^* \simeq 0.3 \text{ m s}^{-1}$.

3.2. The perturbation time development: the weakly nonlinear regime

The linear analysis can explain the appearance of two-dimensional sand waves, but an approach which neglects the interaction among different spatial components of the bottom perturbation cannot model the formation of three-dimensional bottom patterns as those displayed in figure 1. To understand the mechanism which gives rise to three-dimensional sand waves, it is necessary to take into account nonlinear effects and the interaction among the different components of the bottom perturbation. Let us consider values of the parameters close to the critical conditions, i.e. let us assume that the actual value of \hat{r} differs by a small amount from the critical value \hat{r}_c

$$\hat{r} = \hat{r}_c(1 + \epsilon). \quad (3.11)$$

The interaction between two- and three-dimensional harmonic components of the initial perturbation is particularly strong when three components are considered (Craik 1971). The first one corresponds to the most unstable component according to the linear theory and is characterized by a longitudinal wavenumber $\alpha_0 = \alpha$ and a transverse wavenumber γ_0 , which the results indicate would vanish. The other two components have wavenumbers (α_1, γ_1) and (α_2, γ_2) such that $(\alpha_0, \gamma_0) = (\alpha_1, \gamma_1) + (\alpha_2, \gamma_2)$. Under such circumstances, the nonlinear interaction which takes place both in the hydrodynamic and morphodynamic problems, is such that the first perturbation component interacting with the second one generates a sediment transport rate, the divergence of which is spatially distributed as the third component of the bottom perturbation, thus reinforcing it. Similarly, the second component interacting with the third one reinforces the first component and so on. The symmetry of the problem suggests considering $(\alpha_1, \gamma_1) = (\alpha/2, \gamma)$, $(\alpha_2, \gamma_2) = (\alpha/2, -\gamma)$. The above ideas lead us to consider the following structure of the bottom perturbation:

$$h = 1 - \epsilon \sum_{n=0}^2 [A_n e^{i(\alpha_n x + \gamma_n y)} + \text{c.c.}] + O(\epsilon^2). \quad (3.12)$$

The results of the linear stability analysis suggest that, because of (3.11), the growth rate of the bottom perturbation should be of order ϵ . Hence, the amplitudes A_n ($n = 0, 1, 2$) of the perturbation components depend on the slow temporal scale $\mathcal{T} = \epsilon T$ which describes the ‘slow’ growth (or decay) of bottom perturbations averaged over the tide cycle. Then, the solution is expanded in the form

$$\begin{aligned}
(u, v, w, p, Q_x, Q_y) = & \left(u_0, v_0, 0, \frac{\sqrt{g^*}}{\omega^* \sqrt{h_0^*}} P_0, Q_{x0}, Q_{y0} \right) \\
& + \epsilon \sum_{n=0}^2 \left[(u_{1,n}, v_{1,n}, w_{1,n}, \hat{r} P_{1,n}, Q_{x1,n}, Q_{y1,n}) A_n(\mathcal{T}) e^{i(\alpha_n x + \gamma_n y)} + \text{c.c.} \right] \\
& + \epsilon^2 \left\{ [(u_{2,12}, v_{2,12}, w_{2,12}, \hat{r} P_{2,12}, Q_{x2,12}, Q_{y2,12}) A_1(\mathcal{T}) A_2(\mathcal{T}) e^{i(\alpha_0 x + \gamma_0 y)} + \text{c.c.}] \right. \\
& + [(u_{2,02}, v_{2,02}, w_{2,02}, \hat{r} P_{2,02}, Q_{x2,02}, Q_{y2,02}) A_0(\mathcal{T}) \tilde{A}_2(\mathcal{T}) e^{i(\alpha_1 x + \gamma_1 y)} + \text{c.c.}] \\
& + [(u_{2,01}, v_{2,01}, w_{2,01}, \hat{r} P_{2,01}, Q_{x2,01}, Q_{y2,01}) A_0(\mathcal{T}) \tilde{A}_1(\mathcal{T}) e^{i(\alpha_2 x + \gamma_2 y)} \\
& \left. + \text{c.c.}] + \text{o.t.} \right\} + O(\epsilon^3), \tag{3.13}
\end{aligned}$$

where a tilde denotes the complex conjugate of a complex quantity and o.t. stands for other terms which are not relevant for the analysis.

Substituting (3.13) into the problem described in §2 and equating likewise powers of ϵ , the basic tidal current over a flat bed is readily determined at order ϵ^0 . The problem at order ϵ can be solved following the procedure described in the previous section. As already pointed out, because of (3.11), the perturbation components neither amplify nor decay, and the sediment continuity equation reduces to $dA_n/dT = 0$ and states that the functions A_n do not depend on the fast morphodynamic time scale T . Then, it is necessary to consider the problem at $O(\epsilon^2)$ where nonlinear effects are accounted for. Since the local acceleration terms are still neglected by assuming that \hat{r} is sufficiently large ($\hat{r} \gg 1/\epsilon$), the hydrodynamic problems can be solved by means of the same procedure as employed at order ϵ . Then, it is necessary to consider the morphodynamic problem. Because of the chosen values of α_n and γ_n , the nonlinear interactions reproduce the fundamental components of the perturbation. Moreover, since A_n depend on ϵT and because of (3.11), further contributions related to the fundamental components of the bottom perturbation appear in the sediment continuity equation at order ϵ^2 . These contributions are proportional to $dA_n/d\mathcal{T}$ and to A_n , respectively. Following Vittori & Blondeaux (1992) and Roos & Blondeaux (2001), the following amplitude equations are obtained:

$$\frac{dA_0}{d\mathcal{T}} = a_0 A_0 + b_0 A_1 A_2, \quad \frac{dA_1}{d\mathcal{T}} = a_1 A_1 + b_1 A_0 \tilde{A}_2, \quad \frac{dA_2}{d\mathcal{T}} = a_2 A_2 + b_2 A_0 \tilde{A}_1. \tag{3.14}$$

The constants a_n, b_n depend on the parameters of the problem and can be determined by means of straightforward algebra which is not described herein for brevity. The values of a_n and b_n , as function of the parameters of the problem can be found in Vittori & Blondeaux (2008). The system (3.14) is solved numerically using the fourth-order Runge–Kutta method. Even though analytical solutions of the system (3.14) are presented for particular values of a_n, b_n by Craik (1985) and references herein, the general solution of the system (3.14) in closed form is not known. Therefore, it is not possible to provide a general criterion to predict the appearance of three-dimensional sand waves. In the present context, the coefficients a_n, b_n turn out to be real. Moreover, because of the symmetry of the problem, $a_1 = a_2, b_1 = b_2$ and A_1 can be assumed equal to A_2 . In order to study the formation of three-dimensional sand

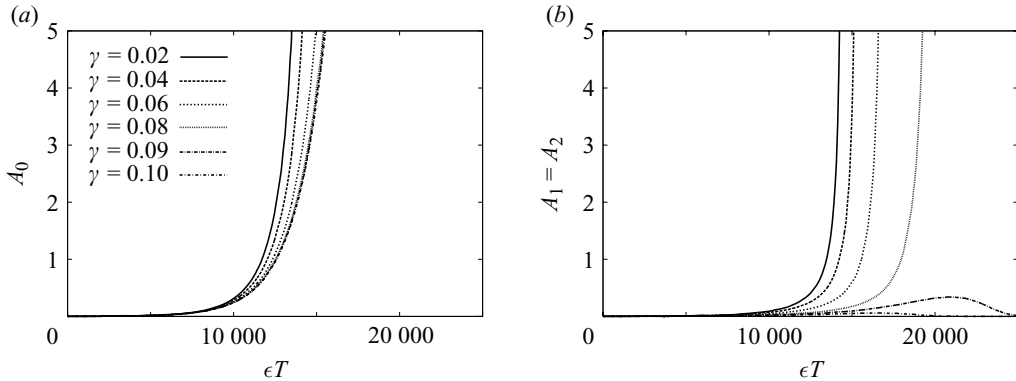


FIGURE 3. Time development of (a) A_0 and (b) $A_1 = A_2$, predicted by the weakly nonlinear analysis for $\hat{r} = 110$, $b/a = 0.2$, $\hat{\Delta} = 2.87 \times 10^{-3}$, $\alpha = 0.39$ and different values of γ .

waves, the functions A_n will be assumed to be real, thus avoiding the analysis of the solution of the system (3.14) in the complex plane. A steady solution of (3.14) exists when $a_0 a_1 / (b_0 b_1)$ is positive. However, a straightforward linear analysis shows that this steady solution is always unstable when a_0 is positive which is the relevant case here, since \hat{r} is larger than \hat{r}_c . Numerical experiments based on the numerical integration of (3.14) do not allow precise quantitative conclusions to be drawn since the solution depends on the initial values of A_n . To simplify the analysis of the behaviour of the system, the initial amplitudes $A_n(0)$ are assumed to be small and the results described in the following have been obtained fixing $A_n(0) = 0.001$. Note that the numerical integration of (3.14) is meaningful until the time development of the bottom can be described by means of a perturbation approach, i.e. until the amplitudes $|A_i|$ remain significantly smaller than ϵ^{-1} . The results obtained show that the qualitative time development of A_i strongly depends on the ratio b/a , i.e. on the ellipticity of the tidal ellipse. For small values of b/a , i.e. for nearly unidirectional tidal currents, and for large values of γ , the nonlinear interaction among the different components of the bottom waviness has no effect on the growth of the bottom perturbation and $A_1 = A_2$ tend to vanish for large values of \mathcal{T} . For small values of γ , the amplitudes of the three-dimensional components grow explosively. However, the fastest growth takes place for $\gamma = 0$. In other words, even though only a fully nonlinear approach can lead to a definitive conclusion, the present weakly nonlinear analysis suggests that, for almost unidirectional tidal currents, the sand waves which tend to appear are two-dimensional. An example of the results is shown in figure 3 which considers the same dimensionless parameters as those of figure 2(a) ($\hat{r} = 110$, $b/a = 0.2$, $\Delta = 2.87 \times 10^{-3}$). Since $\hat{r} = 110$ and $\hat{r}_c = 82$, it follows that $\epsilon = 0.34$.

Three-dimensional bottom patterns are triggered by nonlinear effects when the value of b/a is increased, i.e. when almost circular tides are considered. Figure 2(b) shows the amplification rate Γ_R for the same values of the parameters as those of figure 2(a) but for $b/a = 0.9$. The value of α_c is now equal to about 0.2 and the time development of A_0 and $A_1 = A_2$ is plotted for different values of γ in figure 4. Also in this case, the results obtained show an explosive growth of the three-dimensional components of the bottom perturbation. However, the fastest growth is now observed for a finite value of the transverse wavelength, i.e. when $\gamma = \gamma_{max}$ is equal to about 0.25. Therefore, the bottom forms which are predicted on the basis of the present weakly nonlinear analysis are characterized by a longitudinal wavelength equal to

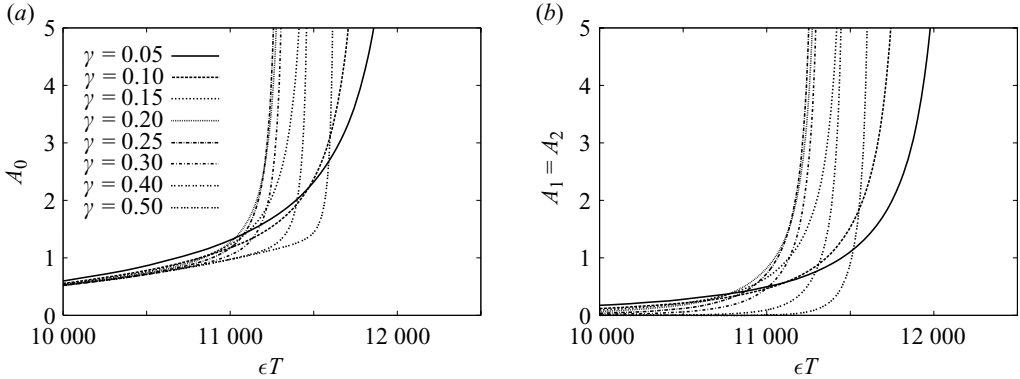


FIGURE 4. Time development of (a) A_0 and (b) $A_1 = A_2$, predicted by the weakly nonlinear analysis for $\hat{r} = 110$, $b/a = 0.9$, $\hat{\Delta} = 2.87 \times 10^{-3}$, $\alpha = 0.2$ and different values of γ .

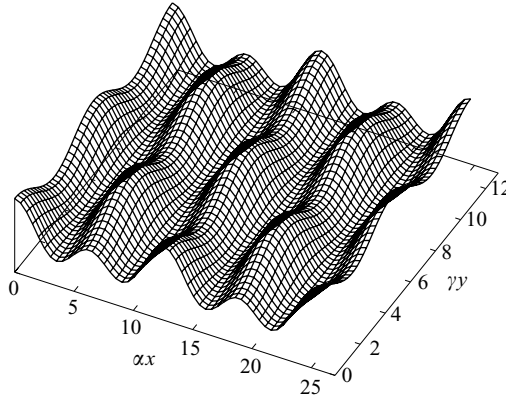


FIGURE 5. Sketch of the bottom topography predicted by the analysis when the growth of three-dimensional bottom perturbations is triggered ($\hat{r} = 110$, $b/a = 0.9$, $\hat{\Delta} = 2.87 \times 10^{-3}$, $\alpha = 0.2$, $\gamma = 0.25$).

$2\pi h_0^*/\alpha_c$ which is close to $30h_0^*$ and a transverse wavelength equal to $2\pi h_0^*/\gamma_{max}$ which is close to $25h_0^*$. The resulting bottom topography is sketched in figure 5. Further results, which have been obtained for different values of the parameters and are not shown herein for brevity, indicate the key role played by the ratio b/a in the formation of three-dimensional sand waves and suggest that three-dimensional bottom forms tend to appear only when b/a is close to one, i.e. for almost circular tides.

4. Conclusions

The investigation of the weakly nonlinear interaction among a triad of resonant harmonic components of a random bottom perturbation has shown that a stability analysis of the flat sea bed forced by tidal currents can explain the appearance of three-dimensional morphological patterns similar to the three-dimensional sand waves observed in the field. In particular, it has been shown that three-dimensional bed forms tend to appear when the ratio between the minor and major axes of the tide ellipse is close to one, i.e. when the tide is almost circular. It is worth pointing out that the present analysis considers only weakly nonlinear effects and therefore it can

describe only the initial stages of the growth of three-dimensional sand waves which subsequently might be modified by fully nonlinear effects. An exhaustive quantitative investigation of the phenomenon in the parameter space is beyond the aims of the present work since the analysis is based on a simple idealized model and significant refinements of the analysis (e.g. a refined description of turbulence characteristics and of sediment transport) are necessary to obtain accurate quantitative predictions of the bottom forms and of the values of the parameters which lead to their appearance.

REFERENCES

- ALLEN, J. R. L. 1984 *Developments in sedimentology*. Elsevier.
- BELDERSON, R. H., JOHNSON, M. A. & KENYON, N. H. 1982 Bedforms. In *Offshore Tidal Sands* (ed. A. H. Stride). Chapman & Hall.
- BESIO, G., BLONDEAUX, P., & FRISINA, P. 2003 A note on tidally generated sand waves. *J. Fluid Mech.* **485**, 171–190.
- BESIO, G., BLONDEAUX, P. & VITTORI, G. 2006 On the formation of sand waves and sand banks. *J. Fluid Mech.* **557**, 1–27.
- BLONDEAUX, P. & VITTORI, G. 2005 Flow and sediment transport induced by tide propagation. Part 2: the wavy bottom case. *J. Geophys. Res.* **110** (C8), C08003
- CRAIK, A. D. D. 1971 Nonlinear resonant instability in boundary layers. *J. Fluid Mech.* **50**, 393–413.
- CRAIK, A. D. D. 1985 *Wave Interactions and Fluid Flows*. Cambridge University Press.
- GERKEMA, T. 2000 A linear stability analysis of tidally generated sand waves. *J. Fluid Mech.* **417**, 303–322.
- HULSCHER, S. J. M. H. 1996 Tidal-induced large-scale regular bed form patterns in a three-dimensional shallow water model. *J. Geophys. Res.* **101**(C9), 20727–20744.
- KNAAPEN, M. A. F. & HULSHER, S. J. M. H. 2002 Regeneration of sand waves after dredging. *Coastal Engng* **46** (4), 277–289.
- KNAAPEN, M. A. F., HULSHER, S. J. M. H., DE VRIEND, H. J. & STOLK, A. 2001 A new type of seabed waves. *Geophys. Res. Lett.* **28**, 1323–1326.
- ROOS, P. 2004 Seabed pattern dynamics and offshore sand extraction. PhD thesis, University of Twente (NL).
- ROOS, P. & BLONDEAUX, P. 2001 Sand ripples under sea waves. Part 4. Tidal ripple formation. *J. Fluid Mech.* **447**, 227–246.
- SEMINARA, G. 1998 Stability and morphodynamics. *Meccanica* **33**, 59–99.
- SLEATH, J. F. A. 1984 *Seabed Mechanics*. John Wiley.
- SOULSBY, R. L. 1983 The bottom boundary layer of shelf seas. In *Physical Oceanography of Coastal and Shelf Seas* (ed. B. Johns), pp. 189–266. Elsevier.
- TAMBRONI, N. & BLONDEAUX, P. 2008 Finite amplitude sand banks. *J. Geophys. Res.* (to appear)
- VITTORI, G. & BLONDEAUX, P. 1992 Sand ripples under sea waves. Part 3. Brick-pattern ripple formation. *J. Fluid Mech.* **239**, 23–45.
- VITTORI, G. & BLONDEAUX, P. 2008 Notes on three-dimensional sand wave formation. Department of Civil, Environmental and Architectural Engineering, University of Genova, Italy, Report 1/08.